ELSEVIER

Quaternary Science Reviews ▮ (▮▮▮▮) ▮▮▮–▮▮▮

QSR

How to combine sparse proxy data and coupled climate models

André Paul*, Christian Schäfer-Neth

DFG Research Center Ocean Margins and Department of Geosciences, University of Bremen, D-28334 Bremen, Germany

Received 2 February 2004; accepted 15 May 2004

Abstract

We address the problem of reconstructing a global field from proxy data with sparse spatial sampling such as the MARGO (multi-proxy approach for the reconstruction of the glacial ocean surface) SST (sea-surface temperature) and $\delta^{18}O_c$ (oxygen-18/oxygen-16 isotope ratio preserved in fossil carbonate shells of planktic foraminifera) data. To this end, we propose to 'assimilate' these data into coupled climate models by adjusting some of their parameters and optimizing the fit. In particular, we suggest to combine a forward model and an objective function that quantifies the misfit to the data. Because of their computational efficiency, earth system models of intermediate complexity are particularly well-suited for this purpose. We used one such model (the University of Victoria Earth System Climate Model) and carried out a series of sensitivity experiments by varying a single model parameter through changing the atmospheric CO_2 concentration. The unanalyzed World Ocean Atlas SST and the observed sea-ice concentration served as present-day targets. The sparse data coverage as implied by the locations of 756 ocean sediment cores from the MARGO SST database was indeed sufficient to determine the best fit. As anticipated, it turned out to be the 365 ppm experiment. We also found that the 200 ppm experiment came surprisingly close to what is commonly expected for the Last Glacial Maximum ocean circulation. Our strategy has a number of advantages over more traditional mapping methods, e.g., there is no need to force the results of different proxies into a single map, because they can be compared to the model output one at a time, properly taking into account the different seasons of plankton growth or varying depth habitats. It can be extended to more model parameters and even be automated.

1. Introduction

The multi-proxy approach for the reconstruction of the glacial ocean surface (MARGO) project will produce various sea-surface temperature (SST) reconstructions from different proxies as well as a reconstruction of $\delta^{18}O_c$ (oxygen-18/oxygen-16 isotope ratio preserved in fossil carbonate shells of planktic foraminifera). It is planned to provide these data at the core locations (Fig. 1) as well as in the form of regularly gridded fields and paleo-maps (see the companion paper by Schäfer-Neth et al., 2005). Such paleo-maps are not only useful for displaying and discussing the data, but also for forcing ocean or atmosphere models.

Examples for simulations of the ocean at the Last Glacial Maximum (LGM) based on the CLIMAP Project Members (1981) SST reconstruction or modifications thereof are given by Seidov et al. (1996), Winguth et al. (1999), Schäfer-Neth and Paul (2001) and Paul and Schäfer-Neth (2003, 2004). In our previous work (Paul and Schäfer-Neth, 2003, 2004) we use the GLAMAP SST reconstruction (Sarnthein et al., 2003a) for the Atlantic Ocean, which as compared to CLIMAP is characterized by 1–2 °C colder tropics and seasonally ice-free Nordic Seas.

On the one hand, classical surface mapping methods of paleo-climate proxy variables make insufficient or no use of (1) the specific properties of each proxy (e.g., different seasons of plankton growth or varying depth habitats) and (2) the dynamical constraints of the ocean circulation, or, more broadly, the coupled ocean–sea-ice–atmosphere system.

*Corresponding author. Tel.: +49-421-218-7189; fax: +49-421-218-7040.

E-mail address: apau@palmod.uni-bremen.de (A. Paul).

0277-3791/$ - see front matter © 2004 Elsevier Ltd. All rights reserved.
doi:10.1016/j.quascirev.2004.05.010

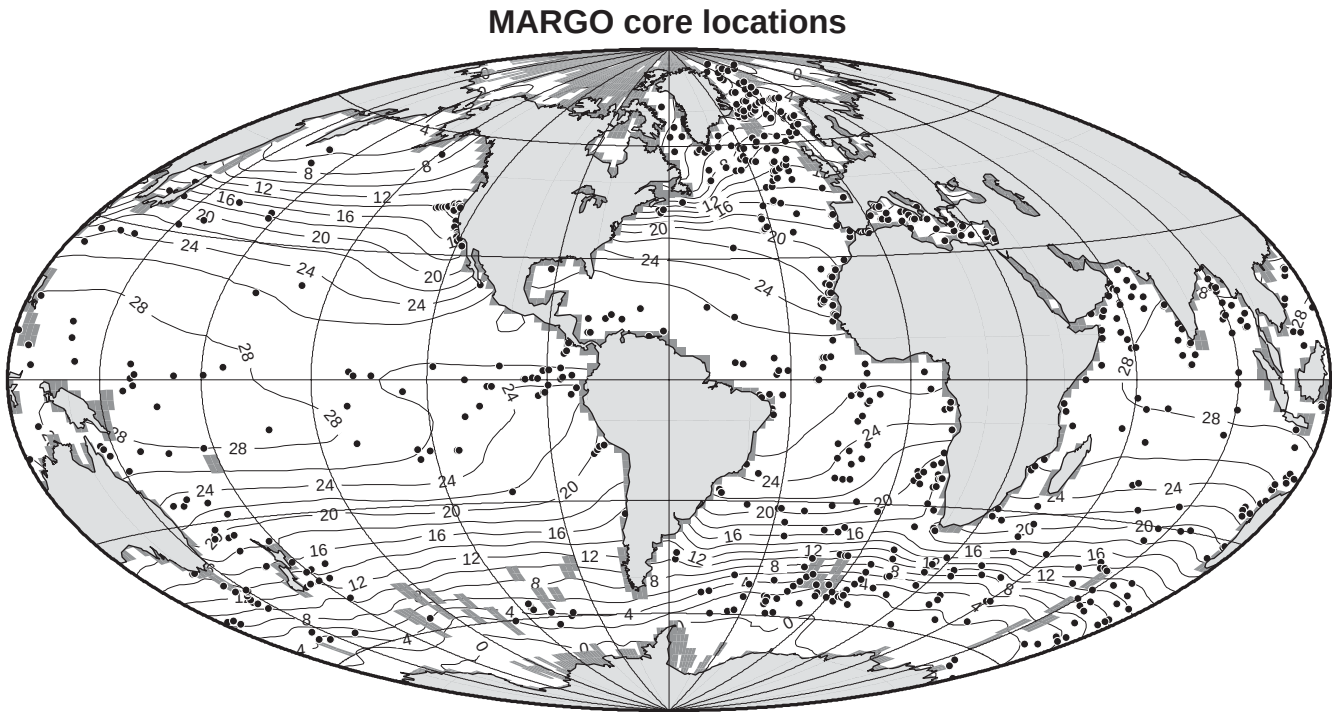

Fig. 1. Unanalyzed annual mean WOA (1998) 10 m temperature (contours at an interval of 2 °C) and distribution of the 756 ocean sediment cores from the MARGO (multi-proxy approach for the reconstruction of the glacial ocean surface) SST (sea-surface temperature) database (circles). The WOA temperature data was smoothed with a cosine arch filter of 2000 km width. Dark gray shading indicates gaps in the original data set. The central meridian of the Hammer equal-area projection is located at 60°W, and the line interval of the geographical grid is 30° (the same map projection is also used in Fig. 2).

On the other hand, coupled climate models do not require the proxy data for forcing and allow for a data–model comparison directly at the core locations (Broccoli and Marciniak, 1996), but their LGM results, although all physically plausible in some sense, are radically different among each other (Mix, 2003). For example, there is no agreement on whether the LGM meridional overturning circulation (MOC) was weaker or stronger than today. Furthermore, these models simulate a wide range of sea-surface temperatures. More generally, they agree with some paleo-data, but are in conflict with some other paleo-data.

We therefore suggest to combine coupled climate models and sparse proxy data and construct an SST map that accommodates best the information obtained from paleo-proxies with the physical constraints of the climate system.

More recently any such data–model combination has been termed 'data assimilation' (Wunsch, 1996), with the general goal to use data in order to improve the performance of numerical models (Hargreaves and Annan, 2002). Here it means finding a set of parameter values such that the model equilibrium solution is best compatible with observational (or proxy-) data.

This method is not entirely new. Even the most comprehensive coupled climate model contains parameterizations of processes that either have not been understood yet from first principles, or that cannot be resolved because of their spatial or temporal scales, and there is some freedom in tuning the associated model parameters. This freedom is used to optimize the fit to present-day climate data. Basically, what we have in mind is to tune a climate model to fit paleo-proxy data.

An earth system model of intermediate complexity is particularly well-suited for this purpose, because it is computationally efficient and can be used to carry out more than one LGM experiment. To illustrate our point of 'assimilating' reconstructed proxy-data into a coupled climate model, we performed a series of experiments with one such model and used the same test data set for present-day SST as in Schäfer-Neth et al. (2005), complemented by a second data set for observed sea-ice concentration. We varied a single model parameter (through changing the atmospheric CO_2 concentration) and left all boundary conditions unchanged. Our strategy could be easily extended to, e.g., the MARGO reconstructions of SST and sea-ice extent, by designing an LGM experiment according to the Paleo-Modelling Intercomparison Project (PMIP) 2 recommendations (http://www-lsce.cea.fr/pmip2/).

2. Methods

We used a coupled climate model, combined it with an explicit objective function that quantified the misfit to the data, selected a parameter which presumably affected the results significantly, performed a series of sensitivity experiments and evaluated the objective function for discrete values of the selected parameter.

2.1. Coupled climate model

We chose the 'UVic Earth System Climate Model' version 2.6, which consists of the Modular Ocean Model (MOM) 2 of the Geophysical Fluid Dynamics Laboratory (GFDL) (Pacanowski, 1996), coupled to an atmospheric energy–moisture balance model (Fanning and Weaver, 1996) and a sea-ice model. We used the sea-ice model in its standard form, in which the thermodynamics is based on the zero-heat capacity formulation by Semtner (1976), together with the lateral growth and melt parameterization by Hibler (1979), and the dynamics is elastic-viscous-plastic (Hunke and Dukowicz, 1997). This particular model version allows for the advection of moisture by monthly winds prescribed from the NCEP reanalysis climatology (Kalnay et al., 1996) and is described in detail by Weaver et al. (2001). The 280 and 365 ppm restart files were kindly provided by Michael Eby (pers. comm.), which enabled us to initialize the model from near-steady states. All experiments were integrated for at least 1000 years, by which time the global air-sea heat flux averaged over 10 years was between 0.009 and 0.135 $\mathrm{W\,m^{-2}}$. This corresponded to a residual trend in the global annual-mean ocean temperature between 0.02 and 0.30 °C per 1000 years.

2.2. Objective function

An objective (or 'cost') function typically characterizes an 'inverse problem' (Wunsch, 1996). Here we combine it with a 'forward model' like the UVic coupled climate model.

The purpose of an objective function F is to provide a measure for the misfit between data and model, and hence it involves the observations (or proxy data) $\mathbf{x}$, the corresponding model output $\mathbf{x}'$ and the model parameters $\mathbf{p}$:

$$F(\mathbf{x},\mathbf{x}',\mathbf{p}) = \sum_{n=1}^{N}\sum_{l=1}^{L} f_{ln}(\mathbf{x},\mathbf{x}',\mathbf{p}). \quad (1)$$

The components f_{ln} of the objective function are taken as sum of squares (e.g., Jentsch, 1991; Hargreaves and Annan, 2002):

$$f_{ln}(\mathbf{x},\mathbf{x}',\mathbf{p}) = \sum_{i}\left(\frac{x_{iln}-x'_{iln}}{g_{iln}}\right)^2. \quad (2)$$

In our case, the number of variables $N = 2$, where $n = 1$ stands for temperature and $n = 2$ for sea-ice concentration. Furthermore, the number of seasons $L = 2$, where $l = 1$ stands for January–February–March (JFM) and $l = 2$ for July–August–September (JAS). The sum on i is over all grid cells that contain data. In particular, $x_{il,n=1}$ refers to the World Ocean Atlas unanalyzed temperature data for 10 m depth (WOA, 1998) and $x_{il,n=2}$ to the Atmospheric Model Intercomparison Project (AMIP) 2 sea-ice concentration data (Taylor et al., 2000).

An important issue is the choice of the weighting factors g_{iln} that are to give each component f_{ln} an approximately equal weight (Jentsch, 1991). We set them such that the objective function became the sum of the individual root-mean square (RMS) seasonal errors, each normalized by the corresponding RMS seasonal contrast of the 365 ppm experiment and squared. The components with $n = 2$ that referred to sea-ice concentration were further multiplied by a factor of 0.12, which is the ratio of the area affected by the AMIP 2 sea-ice concentration data ($43.1\times10^6\ \mathrm{km^2}$) and the area covered by the annual-mean WOA unanalyzed SST data ($361.7\times10^6\ \mathrm{km^2}$).

2.3. Selected parameter

To illustrate our technique, we applied a globally uniform climate forcing

$$Q = \Delta F_{2x}\ln\frac{C}{C_0}$$

to the energy balance at the top of the atmosphere by directly reducing the outgoing longwave radiation (Weaver et al., 2001). Here C is a prescribed atmospheric CO_2 concentration, C_0 some reference level ($C_0 = 350$ ppm) and $\Delta F_{2x} = 5.77\ \mathrm{W\,m^{-2}}$ corresponds to a specified radiative forcing of $4\ \mathrm{W\,m^{-2}}$ for a doubling of CO_2, as estimated from calculations with radiative transfer models (Ramanathan et al., 1987; Hartmann, 1994).

2.4. Series of sensitivity experiments

Usually, the model parameters $\mathbf{p} = (p_1,\ldots)$ would be adjusted within their uncertainty ranges. In our simple example, we tuned the climate forcing Q over a wide range through changing the CO_2 concentration between 200 and 560 ppm (Table 1). This range is much larger than the uncertainty of the radiative transfer scheme, which has been calibrated against satellite and shipboard measurements by Fanning and Weaver (1996).

2.5. Evaluation of the objective function

'Assimilating' (paleo-) data into the coupled climate model now means to evaluate the objective function for

Table 1
List of experiments with atmospheric CO_2 concentration, radiative forcing and equilibrium temperature response (in terms of the global mean surface-air and ocean temperatures, T_a and T_o)

Experiment	pCO_2 (ppm)	Q (W m^{-2})	T_a (°C)	T_o (°C)
1	200	−3.23	11.1	3.3
2	280	−1.28	12.9	3.6
3	365	0.24	14.2	4.2
4	450	1.45	15.2	4.6
5	560	2.67	16.2	5.1

Experiment 5 was a transient experiment, initialized with an atmospheric CO_2 concentration of 280 ppm. The atmospheric CO_2 concentration was increased by 1% per year until the final value of 560 ppm was reached. At this time (i.e., after 70 years of model integration), the global mean surface-air and ocean temperatures were $T_a = 14.9$ °C and $T_o = 3.8$ °C.

discrete values of the selected parameter and search for a minimum. With our choice of the objective function, this is equivalent to the 'least squares method'. To facilitate the comparison with the more traditional mapping methods discussed by Schäfer-Neth et al. (2005), we interpolated the model output as well as the two test data sets (the unanalyzed WOA SST and AMIP2 sea-ice concentration) to a $2^\circ \times 2^\circ$ grid. We computed two types of RMS errors for SST: The first one was based on all unanalyzed WOA data and referred either to the annual mean or the two seasons JFM and JAS. The second one was determined from the annual mean of the unanalyzed WOA data restricted to those $2^\circ \times 2^\circ$ latitude–longitude grid cells that contained at least one of the 756 ocean sediment cores from the MARGO SST database. Furthermore, in presenting or results, we used the same Hammer equal-area map projection as in Schäfer-Neth et al. (2005) (cf. Fig. 1).

3. Results

The simulated annual-mean SST for intermediate atmospheric CO_2 concentrations was generally too cold in the Atlantic Ocean and generally too warm in the Indian and Pacific Oceans (Fig. 2). Regional positive anomalies indicate that the Gulf Stream separated from the coast too far south, and that the water that reached the surface in the major coastal upwelling areas was too warm.

The subtropical and subpolar fronts were reproduced by the coupled climate model, albeit with smaller SST gradients than observed (not shown). In the 365 ppm experiment, the North Atlantic Ocean turned out to be too cold, because the sea ice extended too far equatorwards (cf. Figs. 3 and 4). This in turn was caused by the fact that the NADW was formed slightly too far south (cf. Fig. 5).

For the 365 ppm experiment, the global mean surface-air temperature (Table 1) was close to present-day observations (e.g. 13.84 °C according to the NCEP reanalysis climatology, Kalnay et al., 1996). Comparing the global mean surface-air temperatures for the 280 and 560 ppm experiments, the equilibrium temperature response for a doubling of the atmospheric CO_2 concentration with respect to preindustrial times was 3.3 °C, which is in the range simulated by more comprehensive coupled climate models.

With respect to the present-day climatology, too much sea ice was simulated especially in the Nordic Seas, but also in the Southern Ocean (Figs. 3 and 4). The sea-ice concentration in the 200 ppm experiment as compared to the 365 ppm experiment showed a large expansion during Northern Hemisphere winter down to 50°N (Fig. 3). In contrast, there was still an ice-free region off southern Norway during Northern Hemisphere summer (Fig. 4). In both cases, the simulated sea-ice margins roughly corresponded to the GLAMAP reconstruction (Gersonde et al., 2003; Paul and Schäfer-Neth, 2003; Sarnthein et al., 2003b). During Southern Hemisphere winter, sea ice vastly expanded in the Drake Passage and Atlantic and the Indian sectors of the Southern Ocean.

Fig. 5 shows the MOC in the Atlantic Ocean for LGM and modern atmospheric CO_2 concentrations. The deep circulation is represented by two cells with centers at 1500 and 3500 m depth (in the 200 ppm experiment) and 1500 and 4000 m depth (in the 365 ppm experiment). In the 200 ppm experiment, the formation of North Atlantic Deep Water (NADW) takes place in two latitude bands between 40–50°N and 60–70°N, and the outflow of NADW to the Southern Ocean is 2 Sv ($1\,\mathrm{Sv} = 1 \times 10^6\,\mathrm{m^3\,s^{-1}}$). In contrast, in the 365 ppm experiment, the formation of NADW is concentrated in the 60–70°N latitude band and the outflow of NADW to the Southern Ocean is 12 Sv. The cooling of the tropical SST in the 200 ppm experiment with respect to the 365 ppm experiment amounts to about 3 °C (not shown).

The RMS annual-mean error of SST as a function of latitude for the global ocean was generally smallest for the 365 ppm experiment (left column in Fig. 6), in accordance with the global area-weighted RMS annual-mean errors (cf. Table 2, which can be directly compared to the results presented by Schäfer-Neth et al., 2005). However, in the Atlantic Ocean, the RMS error was smaller for the 450 ppm experiment than for the 365 ppm experiment, while in the Pacific and Indian Oceans, the 280 ppm experiment performed best. The same basic pattern was born out by the unanalyzed WOA data restricted to the MARGO core locations (Table 3 and right column in Fig. 6).

The RMS seasonal SST errors were also generally smallest for the 365 ppm experiment (Table 4). With

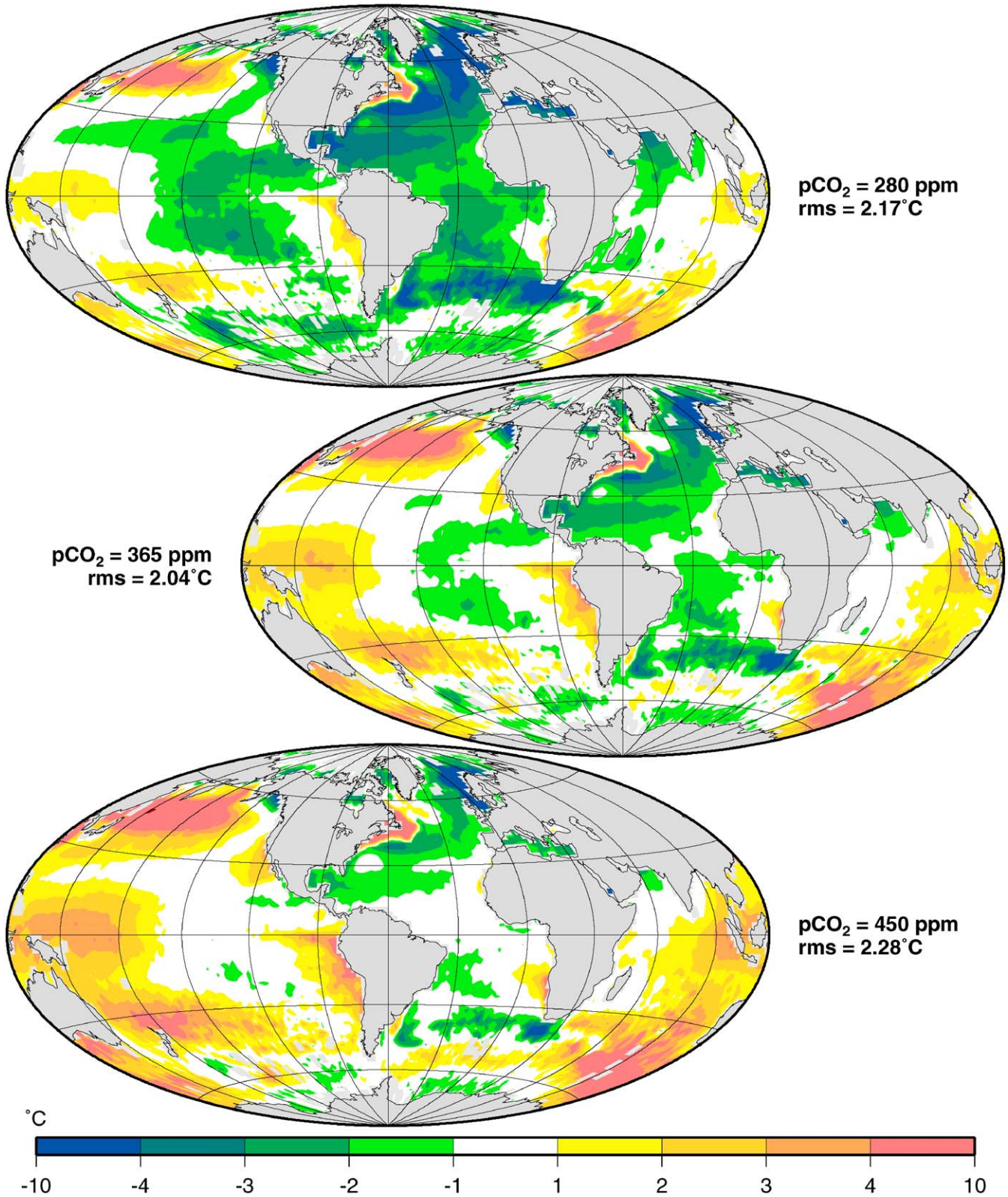

Fig. 2. Difference between the sea-surface temperature as simulated by the UVic coupled climate model for different concentrations of atmospheric CO_2 (all other boundary conditions were unchanged) and the unanalyzed annual-mean WOA (1998) 10 m temperature shown in Fig. 1, in units of °C. Top: 280 ppm. Center: 365 ppm. Bottom: 450 ppm.

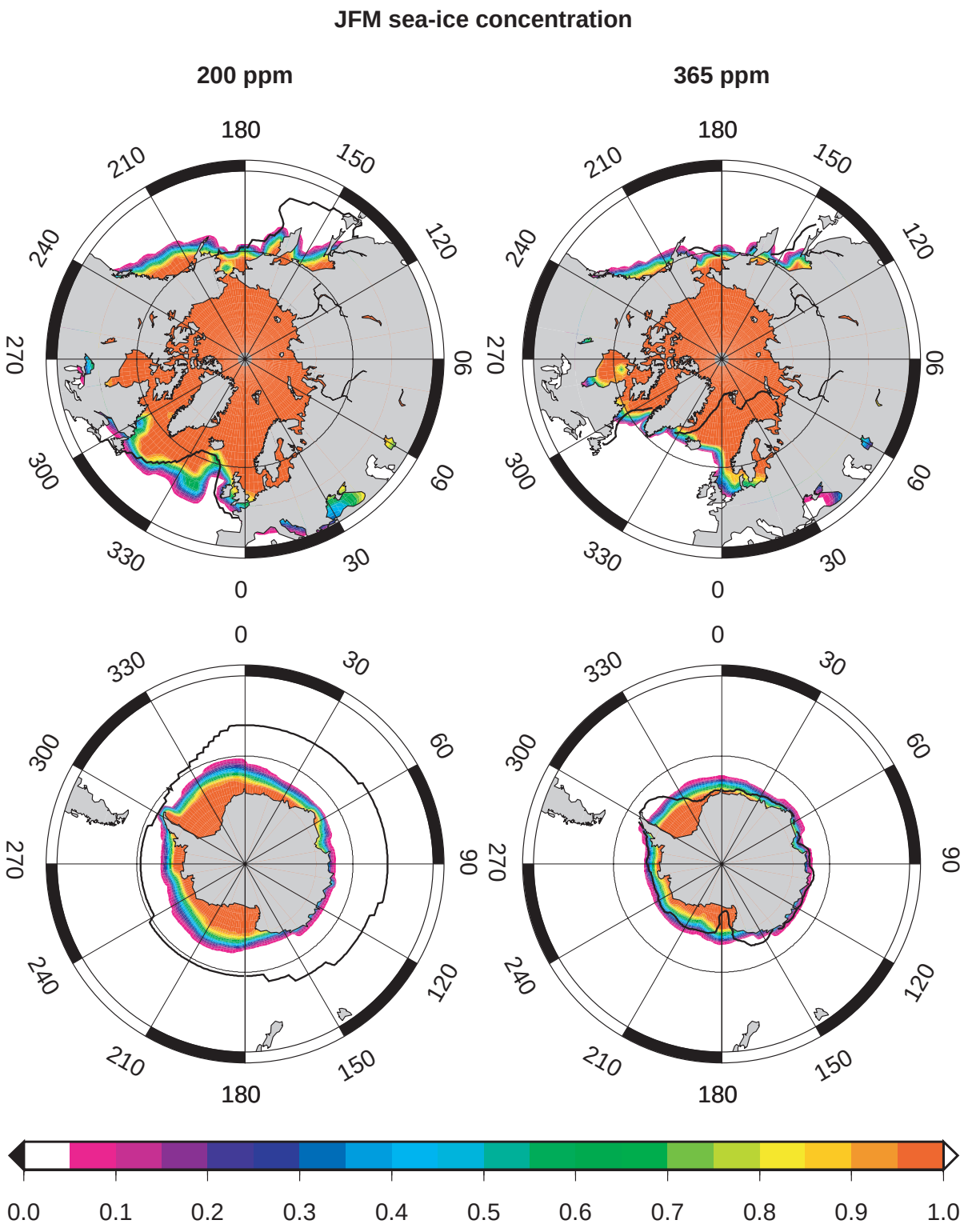

Fig. 3. Simulated sea-ice concentration for JFM (January–February–March) for two different concentrations of atmospheric CO_2, but otherwise unchanged boundary conditions. Left: 200 ppm (value appropriate for the LGM). The thick black lines indicate the sea-ice boundary based on the CLIMAP and GLAMAP reconstructions (Gersonde et al., 2003; Paul and Schäfer-Neth, 2003; Sarnthein et al., 2003b). Right: 365 ppm (present-day value). In the Northern Hemisphere, the thick black line indicates the 50% contour of the AMIP 2 observed climatology for the period of 1979–2001 (Taylor et al., 2000). A 50% contour was used by Sarnthein et al. (2003b) for calibrating their method of reconstructing past sea-ice extent. In the Southern Hemisphere, the thick black line is the 15% contour of the AMIP 2 climatology. A 15% contour is commonly used for indicating present-day sea-ice extent. The polar stereographic map projection (also used in Fig. 4) extends to 40°N in the Northern Hemisphere and 40°S in the Southern Hemisphere, and the line interval of the geographical grid is 30°.

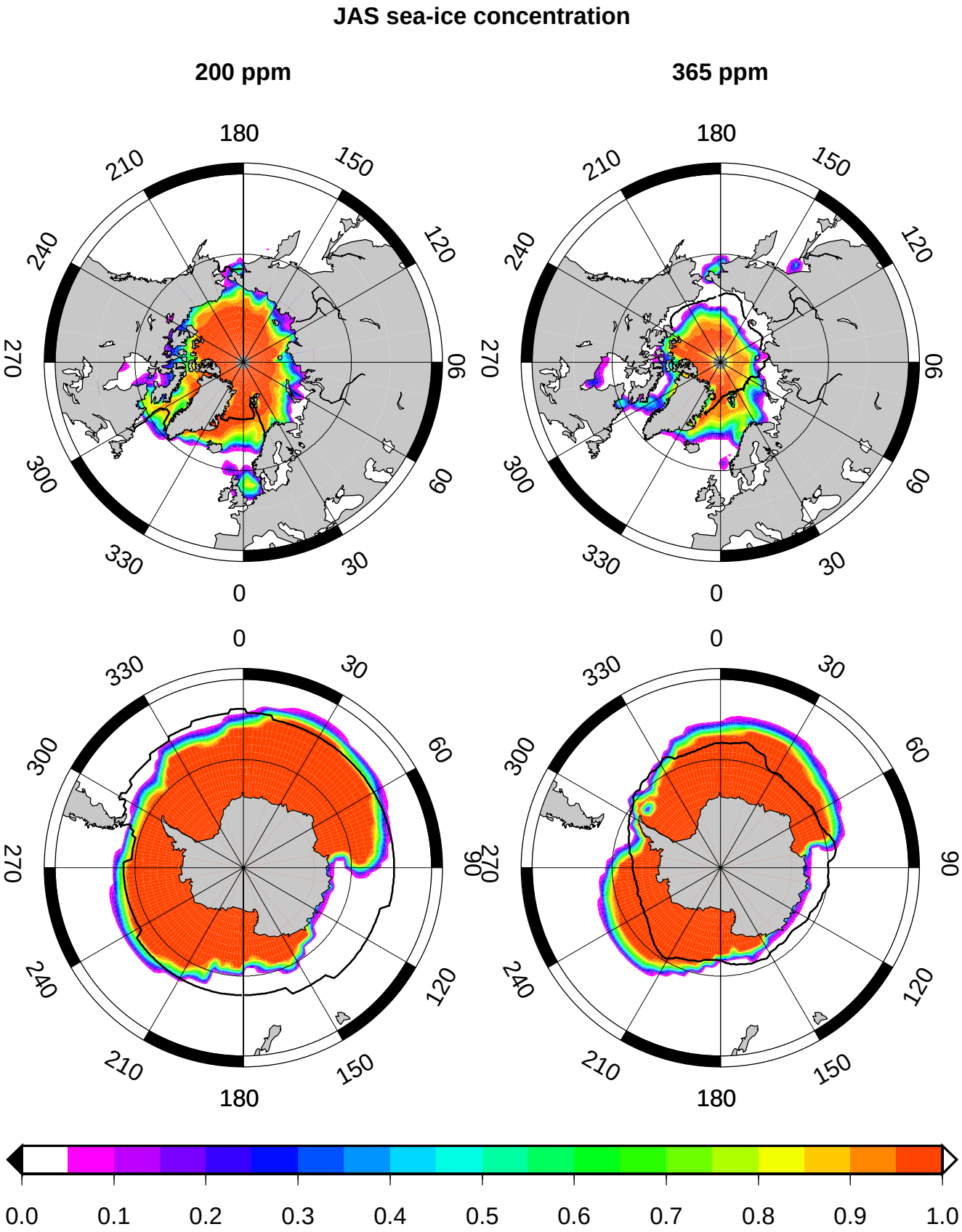

Fig. 4. Simulated sea-ice concentration for JAS (July–August–September) for two different concentrations of atmospheric CO_2, but otherwise unchanged boundary conditions. Left: 200 ppm (value appropriate for the LGM). Right: 365 ppm (present-day value). The thick black lines have a similar meaning as in Fig. 3.

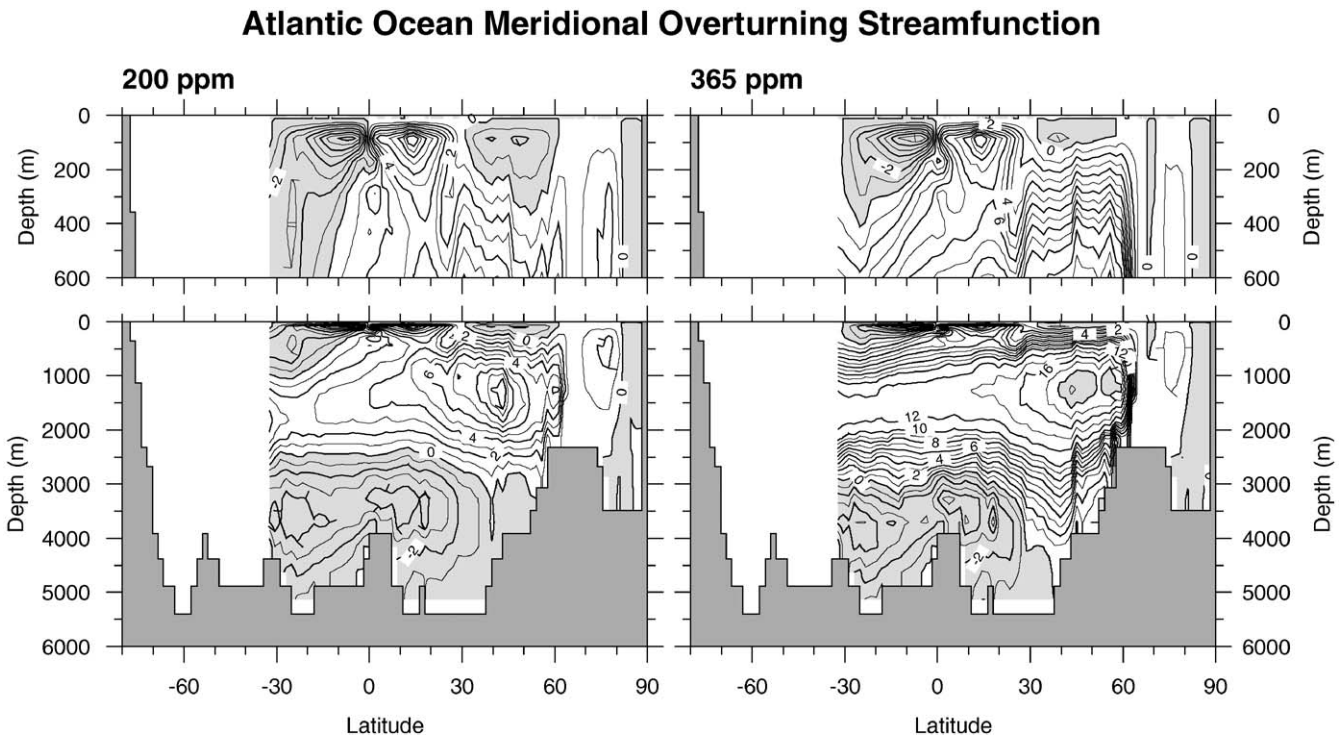

Fig. 5. Vertical meridional overturning streamfunction as simulated by the UVic coupled climate model for two different concentrations of atmospheric CO_2, but otherwise unchanged boundary conditions, in units of Sv ($1\,Sv = 1 \times 10^6\,m^3\,s^{-1}$). Left: 200 ppm. Right: 365 ppm.

respect to sea-ice concentration, the RMS seasonal errors tended to be smaller for the 450 ppm experiment than for the 365 ppm experiment, which reflects that too much sea ice was simulated in the 365 ppm experiment (cf. Figs. 3 and 4). The objective function still attained its minimum value for the 365 ppm experiment (Table 4).

4. Discussion

4.1. Optimum fit

The explicit use of an objective function allowed for a concise measure of the misfit to the target. Accordingly, the 365 ppm experiment showed the best agreement with the present-day test data (Table 4). This did not come as a surprise, because during their development all climate models are carefully tuned to the present-day climate. However, we note that a higher weighting of the sea-ice concentration data relative to the SST data could produce a smaller value of the objective function for the 450 ppm experiment than for the 365 ppm experiment. This shows the sensitivity of the objective function (Eq. (1)) to the choice of the weighting factors (Eq. (2)).

Furthermore, in the 365 ppm experiment the RMS annual-mean SST error reached its minimum value because of a balanced representation of the Atlantic and Indo-Pacific Oceans ('harmony of errors', cf. Table 2 and Fig. 2). The RMS error also concealed large anomalies in regions such as the northern North Atlantic or North Pacific Oceans that are important for deep water formation (Figs. 2 and 6c–f). We could possibly circumvent this problem by choosing a 'minimax' objective function, which would force any minimization procedure to focus on regions with largest data–model discrepancies (LeGrand and Alverson, 2001).

The pre-industrial CO_2 concentration (280 ppm) gave already a noticeably larger deviation from the present-day observations than the 365 ppm experiment, in terms of the objective function as well as the RMS annual-mean SST error; similarly, the 450 ppm experiment. Table 3 shows that we would arrive at the same conclusion if we had to rely on the WOA (1998) data at the MARGO core locations only.

4.2. Comparison to classical mapping methods

Compared to mapping SST data from a density of points given by the location of the MARGO cores using classical methods such as kriging or objective analysis (Schäfer-Neth et al., 2005), the coupled climate model was able to 'reconstruct the modern ocean surface' with an only slightly lower accuracy (the RMS annual-mean error with respect to all available unanalyzed WOA data is 2.04 °C as compared to 1.22 °C for variogram analysis/kriging and 1.56 °C for objective analysis).

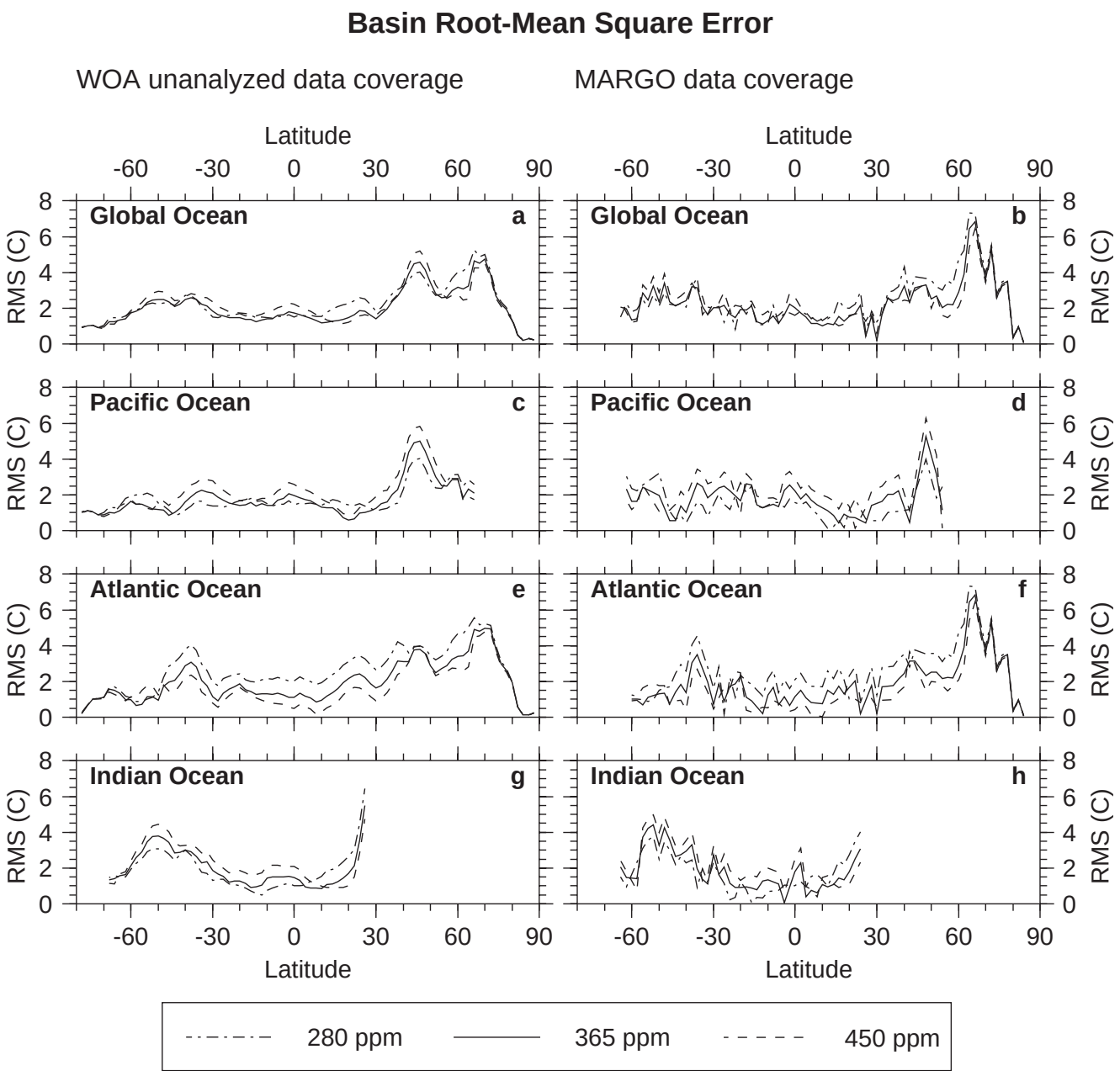

Fig. 6. Zonal-mean distribution of the RMS annual-mean difference between the sea-surface temperature as simulated by the UVic coupled climate model for different concentrations of atmospheric CO_2 (280, 365 and 450 ppm) and the unanalyzed 10 m temperature of the World Ocean Atlas (WOA, 1998), in units of °C, for the global ocean as well as the Pacific, Atlantic and Indian Oceans. Left column: With respect to all available unanalyzed WOA data. Right column: With respect to the unanalyzed WOA data at the MARGO core locations only.

Furthermore, the 'reconstructed' sea-surface conditions are consistent with the fundamental equations of the coupled climate model. Spatial and temporal correlations of the different regions are implicit in these equations. At the chosen resolution of the ocean model, information on ocean currents is exploited and frontal systems are preserved. As an advantage of a coupled climate model (also as compared to an ocean-only model subject to restoring boundary conditions) the sea-ice distribution can be simulated and compared to an independent set of observations. This enabled us to add sea-ice concentration to the objective function.

In addition, there is no need for a sophisticated gridding and mapping of the proxy data at the core locations for other uses than displaying or comparing it. In particular, it is not necessary to extrapolate the proxy data into areas where no sediment cores can be taken, e.g., areas covered by sea ice today, or to make assumptions about seasons during which there is only very little plankton growth and no significant imprint on

Table 2
RMS annual-mean SST differences between the simulated and observed fields at all WOA (1998) unanalyzed data locations (binned into 2° longitude/latitude squares)

Ocean	Atmospheric CO_2 concentration (ppm)				
	200	280	365	450	560
Atlantic	4.29	2.89	2.18	1.83	1.78
Pacific	2.26	1.72	1.85	2.32	2.95
Indian	2.24	1.96	2.23	2.66	3.20
Mediterranean	6.20	4.16	3.10	2.32	1.56
Global	2.97	2.17	2.04	2.28	2.73

Table 3
RMS annual-mean SST differences between the simulated and observed fields restricted to those $2^\circ \times 2^\circ$ latitude–longitude grid cells that contained at least one ocean sediment core from the MARGO SST database

Ocean	Atmospheric CO_2 concentration (ppm)				
	200	280	365	450	560
Atlantic	4.63	2.98	2.34	2.10	2.10
Pacific	1.91	1.55	1.93	2.51	3.20
Indian	2.48	2.07	2.25	2.64	3.16
Mediterranean	6.19	4.10	3.03	2.25	1.48
Global	3.55	2.46	2.24	2.39	2.75

Table 4
Hemispheric RMS seasonal errors (model–data) and seasonal contrasts (model only)

Variable	Hemisphere	Season	Atmospheric CO_2 concentration (ppm)				
			200	280	365	450	560
Sea-surface temperature	NH	JFM	4.13	2.97	2.67	2.72	3.01
		JAS	3.77	2.69	2.64	2.77	3.25
		Model contrast	4.85	4.92	4.90	4.99	4.97
	SH	JFM	2.02	1.87	2.22	2.71	3.27
		JAS	2.81	2.20	2.01	2.20	2.70
		Model contrast	4.32	4.34	4.35	4.27	4.17
Sea-ice concentration	NH	JFM	0.21	0.15	0.14	0.13	0.13
		JAS	0.15	0.13	0.12	0.12	0.12
		Model contrast	0.19	0.18	0.20	0.21	0.18
	SH	JFM	0.11	0.12	0.07	0.07	0.07
		JAS	0.26	0.24	0.19	0.14	0.14
		Model contrast	0.32	0.31	0.28	0.24	0.21
Objective function			2.27	1.35	1.24	1.41	1.90

Here 'NH' stands for 'Northern Hemisphere' and 'SH' for 'Southern Hemisphere'. The value of the objective function is the sum of the individual RMS seasonal differences, each normalized by the corresponding RMS seasonal contrast of the 365 ppm experiment and squared. The components related to sea-ice concentration are further weighted by the ratio of the area affected by the AMIP 2 sea-ice concentration data and the area covered by the annual-mean WOA unanalyzed SST data (which is 0.12, see Methods).

the sedimentary record is left, e.g., winter in the Southern Ocean. The proxy data is only used where and when it is available.

Finally, there is no need to force the results of different proxies into a single map, no matter how desirable such a map would be for other purposes. The

results from the different proxies used in MARGO can be as radically different as those from different coupled climate models. As an advantage of our strategy, they can be compared to the model output one at a time, properly taking into account the different seasons of plankton growth or varying depth habitats. In this way the discrepancies among the different proxies can be addressed and clarified.

A disadvantage of using a coupled climate model for assimilating proxy data is that it is computationally much more demanding than classical mapping methods. Another problem is the ambiguity in minimizing the objective function, which is hidden in the usual forward problem. Model errors might compensate: We might adjust one or a few parameters considered uncertain or critical to match the paleo-data, while actually other parameters may be in cause. To distinguish between multiple solutions, corresponding to multiple sets of model parameters, ultimately requires the computation of the joint 'probability density function' (PDF) of parameter values (Hargreaves and Annan, 2002).

4.3. The 200 ppm experiment

In many ways the 200 ppm experiment came surprisingly close to what is commonly expected from an experiment subject to full LGM boundary conditions. First, it satisfies 'a widespread, if not universal, belief that the LGM circulation was weaker than today', which however, has not been firmly established from plaeotracer data yet (Wunsch, 2003). Second, far from the direct influence of the ice sheets in the high northern latitudes, the main cause of glacial cooling must have been lower levels of atmospheric greenhouse gas concentrations. With a given climate sensitivity of $4\,W\,m^{-2}$ for a doubling of the atmospheric CO_2 concentration, the tropical cooling in the UVic coupled climate model turned out to be 3 °C, which is in accordance with evidence from planktic fauna and flora as well as oxygen isotope measurements (e.g., Crowley, 2000; Schäfer-Neth and Paul, 2004). Third, sea-ice cover vastly expanded, but the Nordic Seas were partly ice-free during summer (Sarnthein et al., 2003b).

The severe reduction of the MOC in the 200 ppm experiment as compared to the 365 ppm experiment is the result of a change in the subtle balance of thermal and haline buoyancy forcing in the Atlantic Ocean. According to the analysis by Schmittner et al. (2002), changes in the atmospheric hydrologic cycle dominate changes in the surface heat flux. We found that these changes caused a reduced convection intensity, decreased SST and reduced evaporation in the North Atlantic Ocean, which in a positive feedback loop led to a further reduction of the MOC. As a result, south of 65°N, evaporation decreased much more than precipitation, which is reflected in the meridional gradients of sea-surface density (Paul and Schäfer-Neth, 2003) and depth-integrated steric height (Schmittner et al., 2002).

To determine absolute LGM circulation rates, additional proxy data is required. Passive, steady-state tracer data alone (such as $\delta^{13}C$) do not suffice, but must be coupled with a 'clock' (LeGrand and Wunsch, 1995). This could be provided by a reconstruction of the LGM density field with accuracy and spatial sampling adequate to infer the paleo-geostrophic shear (Lynch-Stieglitz et al., 1999), or with well-distributed measurements of a radioactive tracer such as ^{14}C (Meissner et al., 2003) or the $^{231}Pa/^{230}Th$ ratio (Yu et al., 1996; Marchal et al., 2000). The absolute strength and associated stability of the glacial circulation are important because they set the stage for understanding rapid climate changes such as the Dansgaard–Oeschger or Heinrich events.

5. Outlook

Regarding the 'assimilation' of real proxy data, our objective function could be adapted to compare the different MARGO SST proxies to the model output one at a time, properly taking into account the different seasons of plankton growth or varying depth habitats. Instead of the observed sea-ice concentration, we could use the reconstructed sea-ice extent for average LGM winter and summer conditions, as depicted in Figs. 3 and 4. By including an isotopic cycle into the UVic coupled climate model, simulating the oxygen isotope ratios $\delta^{18}O_w$ and $\delta^{18}O_c$ and comparing the outcome to the MARGO $\delta^{18}O_c$ reconstruction, we could even exploit the information on the LGM density field that is implicit in the oxygen isotope data (see Discussion). Ideally, we would aim for a good fit to the LGM as well as the present-day data.

The next step would be to extend our method to more than one model parameter, choose a grid of discrete values and search on this grid for a minimum of the objective function. We would select a restricted number of model parameters which are either poorly known or may affect the results significantly (Jentsch, 1991). Parameters related to radiation (e.g., the planetary and atmospheric emissivities, scattering coefficients and planetary albedo, cf. Fanning and Weaver (1996)) dominate the globally averaged climate, while parameters related to dynamics (the coefficients of horizontal diffusion and advection in the atmosphere, the horizontal and vertical diffusion coefficients in the ocean) are mainly important for the redistribution of heat and moisture, and hence the climatic gradients (Jentsch, 1991).

The manual search for the optimum fit could in principle be automated by using inverse methods such as, e.g., nudging, a Kalman filter or the adjoint method

(Wunsch, 1996). Recent examples for the application of inverse methods to paleoceanographic problems are given by Winguth et al. (1999, inverse physical-biogeochemical ocean model), LeGrand and Alverson (2001, inverse ocean box model), Wunsch (2003, inverse dynamical ocean model) and Grieger and Niebler (2003, semi-inverse ocean model).

Each of these inverse methods has its own strengths and weaknesses, e.g., nudging a climate model to data violates such general principles as the conservation of heat and salt, whereas the adjoint method requires finding the inverse ('adjoint') of a complex forward model, which is an extremely tedious and time-consuming task.

Furthermore, a coupled climate model is nonlinear by nature, and the objective function needs no longer have a unique minimum, but 'may come to resemble a chaotic function' with many nearby, or distant, minima, and 'hills, plateaus, and valleys' inbetween (Wunsch, 1996, p. 386). These multiple minima produce predictions that come all very close to the target observations.

A method that overcomes such problems is the Monte Carlo Markov Chain method (Hargreaves and Annan, 2002) based on a Bayesian approach to parameter estimation and the Metropolis-Hastings algorithm. It does not require finding the adjoint and yields the solution to the inverse problem in terms of an estimate for the joint posterior probability density function (PDF), instead of an unique optimum solution. However, at present, this method can only be applied to very efficient climate models. To sample the PDF of the model parameter space of the UVic coupled climate model in its standard form would go beyond the presently available computational resources and require to severely degrade its horizontal and vertical resolution.

6. Conclusion

We addressed the question whether or not a global SST field can be reconstructed from data available at the MARGO core locations. In response to this question, we found that

(1) combining a forward model like the UVic coupled climate model and the use of an objective function quantifies the misfit to the target data in a concise manner,
(2) the sparse MARGO data coverage is indeed sufficient to determine the optimum fit,
(3) the accuracy is comparable to that of classical mapping methods such as kriging or objective analysis.

The strategy of 'assimilating' sparse proxy data (e.g., the MARGO SST reconstruction) into a coupled climate model is free from many restrictions imposed on classical mapping methods by limited sampling density. Finally, we note that our 200 ppm experiment came surprisingly close to what is commonly expected from an experiment subject to full LGM boundary conditions.

Acknowledgements

We thank the participants of the second MARGO workshop (15–17 September 2003, Vilanova i la Geltrú, Spain) for many stimulating discussions. Furthermore, we thank Michael Eby and the Climate Modelling Group at the University of Victoria for providing us with a copy of the UVic coupled climate model. Finally we thank three anonymous referees, as well as Michael Schulz, for their very constructive comments on our original manuscript. This research was funded by the Deutsche Forschungsgemeinschaft (DFG) as part of the DFG Research Center 'Ocean Margins' of the University of Bremen, No. RCOM0185.

References

Broccoli, A.J., Marciniak, E.P., 1996. Comparing simulated glacial climate and paleodata: a reexamination. Paleoceanography 11, 3–14.

CLIMAP Project Members, 1981. Seasonal reconstructions of the Earth's surface at the last glacial maximum. Geological Society of America, Map and Chart Series MC-36, 1–18.

Crowley, T., 2000. CLIMAP SSTs re-revisited. Climate Dynamics 16, 241–255.

Fanning, A.F., Weaver, A.J., 1996. An atmospheric energy–moisture balance model: climatology, interpentadal climate change, and coupling to an ocean general circulation model. Journal of Geophysical Research 101 (D10), 15,111–15,128.

Gersonde, R., Abelmann, A., Brathauer, U., Cortese, G., Fütterer, D., Grobe, H., Niebler, H.-S., Segl, M., Sieger, R., Zielinski, U., 2003. Last glacial maximum sea surface temperature and sea ice extent in the Southern Ocean (Atlantic-Indian sector). a multiproxy approach. Paleoceanography 18, doi 10.1029/2002PA00773.

Grieger, B., Niebler, S., 2003. Glacial South Atlantic surface temperatures interpolated with a semi-inverse ocean model. Paleoceanography 18, doi 10.1029/2002PA000773.

Hargreaves, J.C., Annan, J.D., 2002. Assimilation of paleo-data in a simple Earth system model. Climate Dynamics 19, 371–381, doi 10.1007/s00382-002-0241-0.

Hartmann, D.L., 1994. Global Physical Climatology. Academic Press, San Diego, 411pp.

Hibler, W.D., 1979. A dynamic-thermodynamic sea-ice model. Journal of Physical Oceanography 9, 815–846.

Hunke, E.C., Dukowicz, J.K., 1997. An elastic-viscous-plastic model for sea ice dynamics. Journal of Physical Oceanography 27, 1849–1867.

Jentsch, V., 1991. An energy balance climate model with hydrological cycle. 1. Model description and sensitivity to internal parameters. Journal of Geophysical Research 96 (D9), 17169–17179.

Kalnay, E., Kanamitsu, M., Kistler, R., Collins, W., Deaven, D., Gandin, L., Iredell, M., Saha, S., White, G., Woolen, J., Zhu, Y., Chelliah, M., Ebisuzaki, W., Higgins, W., Janowiak, J., Mo, K.C., Ropelewski, C.A.L., Reynolds, R., Jenne, R., 1996. The NCEP/NCAR reanalysis project. Bulletin of the American Meteorological Society 77, 437–471.

LeGrand, P., Alverson, K., 2001. Variations in atmospheric CO_2 during glacial cycles from an inverse ocean modeling perspective. Paleoceanography 16, 604–616.

LeGrand, P., Wunsch, C., 1995. Constraints from paleotracer data on the North Atlantic circulation during the last glacial maximum. Paleoceanography 6, 1011–1045.

Lynch-Stieglitz, J., Curry, B., Slowey, H., 1999. Weaker Gulf Stream in the Florida Straits during the last glacial maximum. Nature 402, 644–648.

Marchal, O., François, R., Stocker, T.F., Joos, F., 2000. Ocean thermohaline circulation and sedimentary $^{231}Pa/^{230}Th$ ratio. Paleoceanography 15, 625–641.

Meissner, K.J., Schmittner, A., Weaver, A.J., Adkins, J.F., 2003. The ventilation of the North Atlantic Ocean during the last glacial maximum—a comparison between simulated and observed radiocarbon ages. Paleoceanography 18, doi 10.1029/2002PA00762.

Mix, A.C., 2003. Chilled out in the ice-age Atlantic. Nature 425, 32–33.

Pacanowski, R.C.E., 1996. MOM 2. Documentation, user's guide and reference manual. Technical Report 3.2, GFDL Ocean Group, GFDL, Princeton, New Jersey.

Paul, A., Schäfer-Neth, C., 2003. Modeling the water masses of the Atlantic Ocean at the last glacial maximum. Paleoceanography 18, doi 10.1029/2002PA000783.

Paul, A., Schäfer-Neth, C., 2004. The Atlantic Ocean at the last glacial maximum: 2. Reconstructing the current systems with a global ocean model. In: Wefer, G., Mulitza, S., Ratmeyer, V. (Eds.), The South Atlantic in the Late Quaternary: Reconstruction of Material Budgets and Current Systems. Springer, Berlin, Heidelberg, pp. 549–583.

Ramanathan, V., Callis, L., Cess, R., Hansen, J., Isaksen, I., Kuhn, W., Lacis, A., Luther, F., Mahlman, J., Reck, P., Schlesinger, M., 1987. Climate-chemical interactions and effects of changing atmospheric trace gases. Reviews of Geophysics 25, 1441–1482.

Sarnthein, M., Gersonde, R., Niebler, S., Pflaumann, U., Spielhagen, R., Thiede, J., Wefer, G., Weinelt, M., 2003a. Preface: glacial Atlantic Ocean mapping (GLAMAP-2000). Paleoceanography 18, doi 10.1029/2002PA00769.

Sarnthein, M., Pflaumann, U., Weinelt, M., 2003b. Past extent of sea ice in the northern North Atlantic inferred from foraminiferal paleotemperature estimates. Paleoceanography 18, doi 10.1029/2002PA00771.

Schäfer-Neth, C., Paul, A., 2001. Circulation of the glacial Atlantic: a synthesis of global and regional modeling. In: Schäfer, P., Ritzrau, W., Schlüter, M., Thiede, J. (Eds.), The northern North Atlantic: a changing environment. Springer, Berlin, Heidelberg, pp. 441–462.

Schäfer-Neth, C., Paul, A., 2004. The Atlantic Ocean at the last glacial maximum: 1. Objective mapping of the GLAMAP sea-surface conditions. In: Wefer, G., Mulitza, S., Ratmeyer, V. (Eds.), The South Atlantic in the Late Quaternary: Reconstruction of Material Budgets and Current Systems. Springer, Berlin, Heidelberg, pp. 531–548.

Schäfer-Neth, C., Paul, A., Mulitza, S., 2005. Perspectives on mapping the MARGO reconstructions by variogram analysis/kriging and objective analysis. Quaternary Science Reviews, this issue.

Schmittner, A., Meissner, K.J., Eby, M., Weaver, A.J., 2002. Forcing of the deep ocean circulation in simulations of the last glacial maximum. Paleoceanography 17, 26–35.

Seidov, D., Sarnthein, M., Stattegger, K., Prien, R., Weinelt, M., 1996. North Atlantic ocean circulation during the last glacial maximum and a subsequent meltwater event: a numerical model. Journal of Geophysical Research C 101, 16,305–16,332.

Semtner, A.J., 1976. A model for the thermodynamic growth of sea ice in numerical investigations of climate. Journal of Physical Oceanography 6, 379–389.

Taylor, K., Williamson, D., Zwiers, F., 2000. The sea surface temperature and sea ice concentration boundary conditions for AMIP II simulations, http://www-pcmdi.llnl.gov/pcmdi/pubs/ab60.html. Technical Report, Program for Climate Model Diagnosis and Intercomparison, Lawrence Livermore National Laboratory.

Weaver, A.J., Eby, M., Wiebe, E.C., Bitz, C.M., Duffy, P.B., Ewen, T.L., Fanning, A.F., Holland, M.M., MacFadyen, A., Matthews, H.D., Meissner, K.J., Saenko, O., Schmittner, A., Wang, H., Yoshimori, M., 2001. The UVic earth system climate model: model description, climatology, and applications to past, present and future climates. Atmosphere-Ocean 39, 361–428.

Winguth, A.M.E., Archer, D., Duplessy, J.C., Maier-Reimer, E., Mikolajewicz, U., 1999. Sensitivity of paleonutrient tracer distributions and deep-sea circulation to glacial boundary conditions. Paleoceanography 14, 304–323.

WOA, 1998. World ocean atlas 1998, http://www.nodc.noaa.gov/oc5/woa98.html. Technical Report, National Oceanographic Data Center, Silver Spring, MD.

Wunsch, C., 1996. The Ocean Circulation Inverse Problem. Cambridge University Press, New York, 442pp.

Wunsch, C., 2003. Determining paleoceanographic circulations, with emphasis on the last glacial maximum. Quaternary Science Reviews 22, 371–385.

Yu, E.-F., Francois, R., Bacon, M.P., 1996. Similar rates of modern and last-glacial ocean thermohaline circulation inferred from radiochemical data. Nature 379, 689–694.